Synchronous interhemispheric Holocene climate trends in the tropical Andes

Pratigya J. Polissar[a,1], Mark B. Abbott[b], Alexander P. Wolfe[c], Mathias Vuille[d], and Maximiliano Bezada[e]

[a]Division of Biology and Paleo Environment, Lamont-Doherty Earth Observatory of Columbia University, Palisades, NY 10964; [b]Department of Geology and Planetary Science, University of Pittsburgh, Pittsburgh, PA 15260; [c]Department of Earth and Atmospheric Sciences, University of Alberta, Edmonton, AB, Canada T6G 2E3; [d]Department of Atmospheric and Environmental Sciences, State University of New York, Albany, NY 12222; and [e]Departamento de Ciencias de la Tierra, Universidad Pedagógica Experimental Libertador, El Pararaîso, Caracas, Venezuela

Edited by Thure E. Cerling, University of Utah, Salt Lake City, UT, and approved July 23, 2013 (received for review November 12, 2012)

Holocene variations of tropical moisture balance have been ascribed to orbitally forced changes in solar insolation. If this model is correct, millennial-scale climate evolution should be antiphased between the northern and southern hemispheres, producing humid intervals in one hemisphere matched to aridity in the other. Here we show that Holocene climate trends were largely synchronous and in the same direction in the northern and southern hemisphere outer-tropical Andes, providing little support for the dominant role of insolation forcing in these regions. Today, sea-surface temperatures in the equatorial Pacific Ocean modulate rainfall variability in the outer tropical Andes of both hemispheres, and we suggest that this mechanism was pervasive throughout the Holocene. Our findings imply that oceanic forcing plays a larger role in regional South American climate than previously suspected, and that Pacific sea-surface temperatures have the capacity to induce abrupt and sustained shifts in Andean climate.

Venezuela | Bolivia | Caribbean | El Niño-Southern Oscillation | Milankovitch

Variations in solar insolation driven by the precession of the equinoxes have been invoked as the determinant factor modulating tropical climate on millennial timescales (1–5). Humid conditions prevail in the hemisphere where perihelion (minimum earth–sun distance) coincides with the summer wet season (June–August in the northern hemisphere, December–February in the southern hemisphere), whereas the opposite hemisphere experiences a drier climate. The proposed mechanism calls for enhanced solar heating, convection, and rainfall during the wet season when it coincides with perihelion. This mechanism is supported by a number of South American Holocene paleoclimate records in the southern hemisphere. Runoff from the Amazon Basin (1), evaporation in Peruvian lakes (2), speleothem $\delta^{18}O$ (3, 6, 7), ice cores (4, 8), and lake sediment records (5) all suggest these regions became wetter as summer insolation increased during the Holocene. Additional support for this mechanism comes from reduced precipitation in regions that are dynamically linked to convection in the southern hemisphere tropics, such as the Nordeste of Brazil (9).

In contrast to the southern hemisphere, evidence for precessional forcing of Holocene climate in northern South America remains equivocal, and there appear to be more complex spatial patterns of climate evolution that are not consistent between available marine and terrestrial paleoclimate records. Marine sediments off the Venezuelan coast (10–11 °N) indicate a decrease of terrigenous (continental) sedimentation during the Holocene, providing evidence for reduced precipitation with decreasing northern hemisphere summer insolation (10). However, terrestrial Holocene paleorecords from low-altitude Andean sites do not support a direct insolation forcing mechanism. For example, results from Lake Valencia in northern Venezuela [10° 11′ N, 67° 43′ W, 402 m above sea level (a.s.l.)] indicate arid conditions during the early Holocene, a humid interval during the middle Holocene, and a return to arid conditions in the late Holocene (11, 12). This arid–humid–arid sequence is at odds with the marine evidence for precessional forcing of climate, suggesting either a sharp climatic boundary between coastal and inland Venezuela, or perhaps a more complex control over terrigenous geochemical indicators in the marine record (13, 14) (*SI Text* and Fig. S1).

Here we present a unique multiproxy record of Holocene climate from Laguna Blanca in the Venezuelan Andes, which is strategically located to test whether precessional forcing resulted in antiphased climate changes in the northern and southern hemispheres of the Cordillera, and resolve the discrepancy between terrestrial and marine climate histories. Laguna Blanca (8° 20′ N, 71° 47′ W, 1,620 m a.s.l.; Fig. 1 and Fig. S2) is a small shallow lake in an unglaciated watershed where sediment lithology and geochemistry offer first-order proxies for changes in lake level and hence regional moisture balance. We use sediment organic content, dry density, and magnetic susceptibility (MS) to characterize sediment lithology, constrained by a robust chronological framework based on 11 calibrated accelerator-mass spectrometric (AMS) radiocarbon ages from terrestrial macrofossils and bulk sediment (*SI Text* and Fig. S3). Carbon/nitrogen (C/N) molar ratios distinguish terrestrial (C/N > ~30) from aquatic (C/N < ~15) organic matter. Previous results documented that a humid period with overflowing lake levels coincided with glacier advances in the Venezuelan Andes during the Little Ice Age (15). Here we extend this record back to 11,000 y before present (BP) to document shifts in lake level that reflect millennial-scale patterns of Andean climate evolution.

Results and Discussion

During the early Holocene, finely laminated lacustrine sediments accumulated in Laguna Blanca, dominated by autochthonous organic matter and minerogenic influxes from the catchment, together resulting in high sediment accumulation rates (Fig. 2). This style of deposition results from humid conditions that prevailed between 11,000 and 8,200 y BP. However, an intense drought punctuated this interval between ~9,100 and 8,500 BP, as indicated by a hiatus in sediment accumulation. This arid interval is also preserved in nearby Laguna Brava (8° 19′ N, 71° 50′ W, 2,380 m a.s.l.; Fig. 1), indicating a period of sustained regional drought. The calibrated radiocarbon age of lacustrine sediments from Laguna Brava immediately overlying the desiccation surface (Table S1) dates the return to wetter conditions at 8,410 y BP. The cause of this drought remains uncertain, as it predates the 8,200-y event identified in many tropical and high latitude records (16).

Author contributions: P.J.P., M.B.A., and A.P.W. designed research; P.J.P., M.B.A., A.P.W., and M.B. performed research; P.J.P., M.B.A., A.P.W., M.V., and M.B. analyzed data; and P.J.P., M.B.A., A.P.W., and M.V. wrote the paper.

The authors declare no conflict of interest.

This article is a PNAS Direct Submission.

[1]To whom correspondence should be addressed. E-mail: polissar@ldeo.columbia.edu.

This article contains supporting information online at www.pnas.org/lookup/suppl/doi:10.1073/pnas.1219681110/-/DCSupplemental.

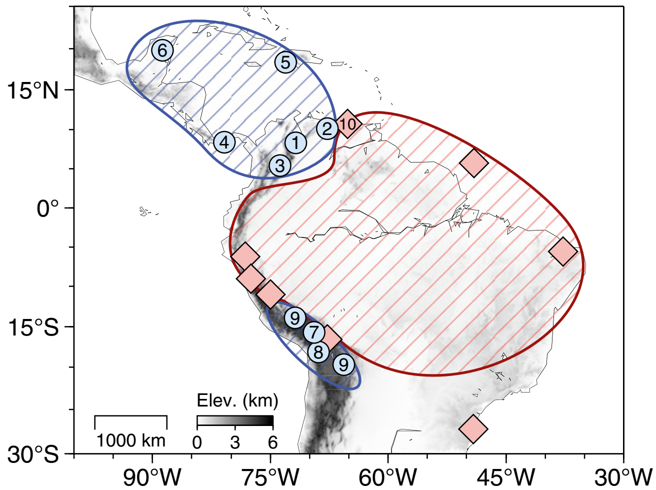

Fig. 1. South American topography and the location of paleoclimate records discussed in the text: 1, Laguna Blanca, Venezuela; 2, Lake Valencia, Venezuela; 3, Lake Fuquene, Colombia; 4, Lake La Yeguada, Panama; 5, Lake Miragoane, Haiti; 6, Lake Chichancanab, Yucatan Mexico; 7, Lake Titicaca, Peru/Bolivia; 8, Nevado Sajama, Bolivia; 9, small lakes in the Cordillera Réal, Bolivia; 10, Cariaco Basin. Blue circled sites and patterned areas are in-phase with Laguna Blanca while red-diamond sites and patterned areas are more coherent with solar insolation.

Lake levels dropped markedly in Laguna Blanca during the middle Holocene (8,200–2,000 y BP), as evidenced by decreased rates of sediment accumulation, elevated organic carbon content, abundant subfossil littoral macrophytes, and a marked decline in mineral sedimentation. Mire accumulation peaked between 7,000 and 4,000 y BP, as indicated by high organic carbon concentrations and correspondingly terrestrial C/N ratios. Bracketing this interval are periods of more variable lake levels that mark transitions into and out of the most arid intervals of the middle Holocene (8,000–7,000 and 4,000–2,000 y BP). Higher lake levels stabilized around 2,000 y BP, when increased mineral content and aquatic organic matter signify a return to lacustrine sedimentation. High lake levels culminated in the wettest conditions of the Holocene during the Little Ice Age (700–130 BP), when mineral sedimentation peaked in the lake system (15).

The timing and abruptness of Holocene moisture balance changes in Laguna Blanca differs fundamentally from that predicted by orbital insolation forcing. During the early Holocene, stronger seasonality from enhanced summer and reduced winter insolation in the northern tropics (Fig. S4) are thought to have enhanced the summer wet season by shifting precipitation patterns northward (10). In this scenario, the decreasing seasonality of insolation in the middle and late Holocene would have weakened this mechanism, ultimately leading to progressively more arid conditions. Although the early Holocene wet period and middle Holocene arid intervals inferred from Laguna Blanca are broadly consistent with northern hemisphere insolation forcing, the abrupt character of climate transitions coupled with the increased moisture balance during the late Holocene call into question the dominant role of insolation in modulating Holocene climate variability (Fig. 3, *SI Text*).

Interhemispheric Comparisons. Further evidence against a simple response to insolation in the outer tropics is provided by the coherence between additional Andean paleorecords from the northern and southern hemispheres. Paleolimnological results from Lake Titicaca (15° 45′ S, 69° 25′ W, 3,810 m a.s.l.) document a period of higher lake levels during the early Holocene that coincides with the wet interval in the Venezuelan Andes (Fig. 3). Lake Titicaca was fresh and overflowing 10,000–8,000 y BP (17), despite a minimum in insolation seasonality that should have decreased precipitation and increased evaporation. During

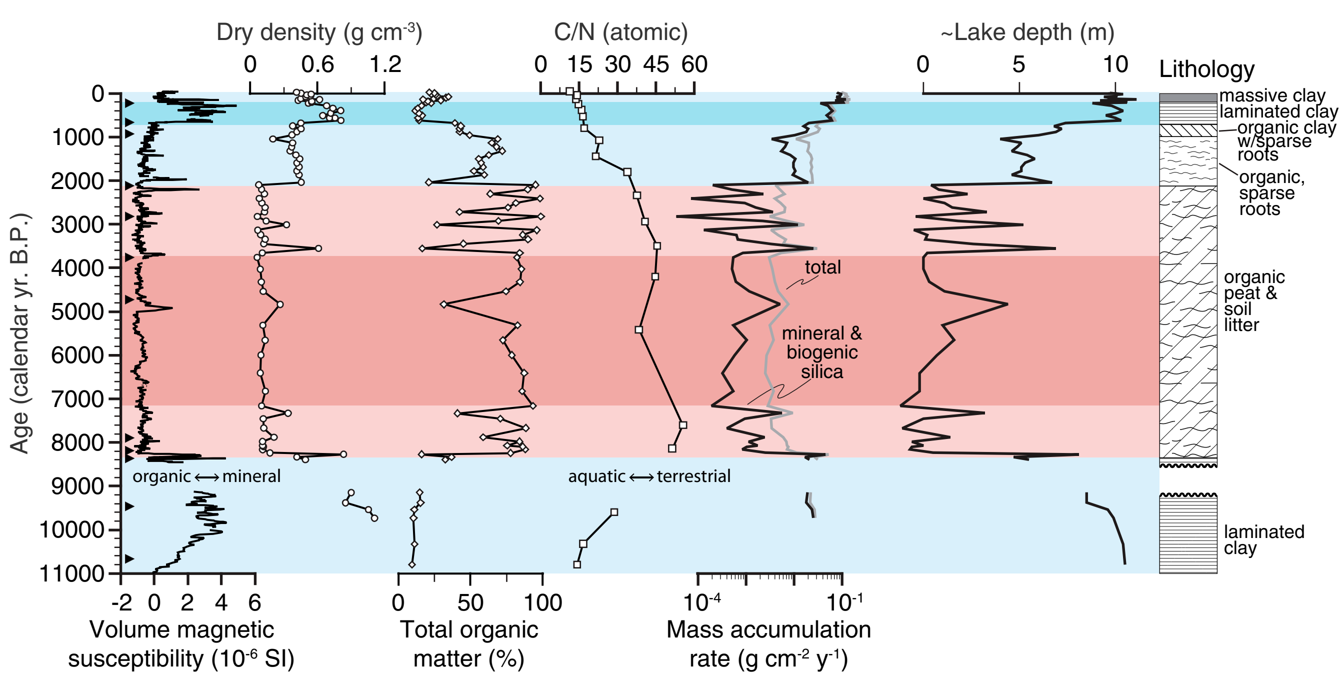

Fig. 2. Stratigraphy, sediment physical and geochemical properties, and lake-level reconstruction from Holocene sediments of Laguna Blanca. Triangles denote calibrated radiocarbon ages used for chronologic control (*SI Text*). Note log scale for accumulation rates. An approximate measure of lake depth was calculated from the sediment type determined by the first principle component of dry density, organic matter, C/N, and mineral accumulation scaled to the lake depth necessary for overflow (10 m), current lake depth (5 m), and the cutoff lake depth necessary for abundant soil litter accumulation (<1 m) (*SI Text* and Figs. S7 and S8). Blue and red shading indicates humid and arid intervals, respectively.

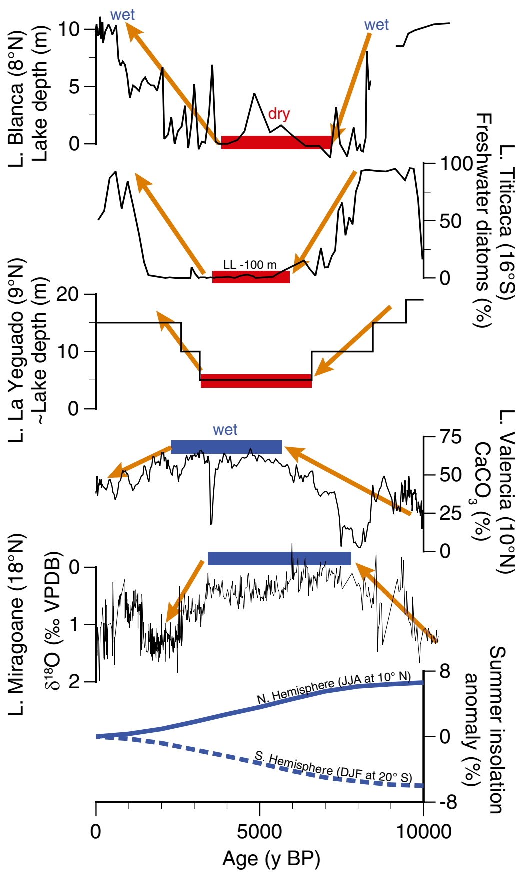

Fig. 3. Holocene paleoclimate records from the northern and southern Neotropics. Lake Titicaca freshwater diatoms reflect salinity (17), whereas a lowstand (red horizontal line) observed in sediment cores and inferred from seismic reflection surveys and sediment geochemistry (19, 20) indicates the driest interval. Lake La Yeguado water levels are inferred from the timing of sediment deposition in cores at different depths, the abundance of epiphytic diatoms that record flooding of a shallow shelf, and the influx of phytoliths that reflect allochthonous delivery to the lake (32). Lake Valencia authigenic carbonate reflects positive lake water balance as corroborated by diatom, pollen, and isotopic data (11, 12, 31). Lake Miragoane ostracode $\delta^{18}O$ reflects the evaporative enrichment of lake water (38, 39). None of these records track the summer wet season insolation (as % anomaly from the present) at their respective latitude.

the middle Holocene, Lake Titicaca lowered and became more saline by evaporative enrichment, in broad synchrony with the advent of mire sedimentation in Laguna Blanca. More specifically, the driest interval in Lake Titicaca, when water levels fell ~100 m below modern levels and the Huinamarca basin was completely dry, occurred between 7,000 and 4,000 y BP (18–20). This coincides with the most arid interval inferred from Laguna Blanca. Lake Titicaca freshened and Laguna Blanca lake levels increased markedly after 2,000 y BP, producing conditions that have been sustained to the present. The spectacular Holocene moisture balance shifts recorded in Lake Titicaca are also registered by isotopic and sedimentological records from glacially fed headwater lakes in the Bolivian Andes (21). Alpine glaciers disappeared from high-elevation watersheds in the Cordillera Réal between 8,500 and 2,200 y BP, indicating sustained regional aridity over this protracted interval (22).

These comparisons reveal a pattern of Holocene paleohydrology in the outer tropics of South America that is broadly synchronous between the hemispheres, and thus cannot be mediated by precessional forcing alone. In-phase behavior across the equator is not predicted from insolation forcing because precession changes are 180° out of phase between the northern and southern hemispheres. Furthermore, Holocene insolation patterns evolve gradually over millennia, and are not anticipated to induce the sudden, threshold-type hydrological responses indicated here (Fig. 3). Therefore, different mechanisms are required to synchronize interhemispheric climatic and hydrologic variability between these regions.

Today, sea-surface temperatures (SSTs) in the equatorial Pacific perturb atmospheric circulation patterns and cause coherent, in-phase interannual variability in both hemispheres (23, 24). We suggest that similar mechanisms have operated on millennial timescales, resulting in coherent interhemispheric moisture balance changes in the outer tropics of both hemispheres. Although SSTs in the Caribbean and tropical Atlantic may also influence climate in these regions, their effects are deemed secondary in the outer tropical Andes, as detailed below. While other factors may play a role locally, synchronization of climate in the outer tropics requires large-scale changes in atmospheric circulation that are coherent between hemispheres and persistent across both the boreal and austral seasons. We hypothesize that the evolution of variability of eastern equatorial Pacific SSTs provides such a mechanism. This is supported by (*i*) the modern relationship between equatorial Pacific SSTs and precipitation over these regions (25), (*ii*) records of tropical Pacific Holocene SST evolution, and (*iii*) the coherent fingerprints of Holocene climate evolution in the Neotropics.

Correlating South American Precipitation with SSTs. Modern climate data from the Venezuelan Andes demonstrate the pervasive influence of equatorial Pacific SSTs. Increased precipitation, the primary driver of Laguna Blanca water levels, occurs in the Venezuelan Andes when SSTs are below average in the eastern equatorial Pacific and tropical south Atlantic, and above average in the Caribbean (24). The correlation of precipitation anomalies with equatorial Pacific SST variability (Niño 3.4 index) is strongly negative over the Venezuelan Andes, indicating that higher lake levels would accompany cold SSTs and vice versa (Fig. 4). In support of this inference, available precipitation time series from meteorological stations in the Venezuelan Andes correlate with equatorial Pacific SSTs in a highly coherent pattern that is typical of El Niño-Southern Oscillation (ENSO) variability (26).

Historical water level records from Lake Titicaca also demonstrate a persistent influence of tropical Pacific SSTs on regional water balance. Hydrologic modeling indicates that Lake Titicaca's water balance is more strongly mediated by precipitation than net evaporation (27). Therefore, as with Laguna Blanca, Holocene lake-level histories primarily record changes in precipitation. Precipitation in the Titicaca watershed is strongly modulated by equatorial SSTs in the tropical Pacific (28, 29), through perturbations to easterly winds that deliver moisture to the high Andes. Cold SSTs in the eastern equatorial Pacific and stronger meridional SST gradients strengthen easterly flow over South America during the austral summer. These winds entrain boundary layer moisture from the Amazon basin and deliver it to the high Andes, enhancing precipitation. This mechanism operates on intraseasonal and longer timescales, as illustrated by the negative correlation between equatorial Pacific SSTs and precipitation in the Titicaca region (Fig. 3).

We evaluate the influence of various ocean regimes on South American climate by mapping correlations between gridded precipitation datasets and SST time series from the tropical Pacific, Atlantic, and Caribbean Oceans (Fig. 4 and *SI Text*). Mean annual SSTs from the Niño 3.4, Caribbean, north Atlantic, and south Atlantic sectors (Fig. S5) were assessed spatially in relation to South American gridded rainfall data (30). The results demonstrate that the geographic patterns in proxy records is best accounted for by Pacific Ocean SSTs (i.e., the Niño 3.4 index). The sign of these correlations is opposite between the

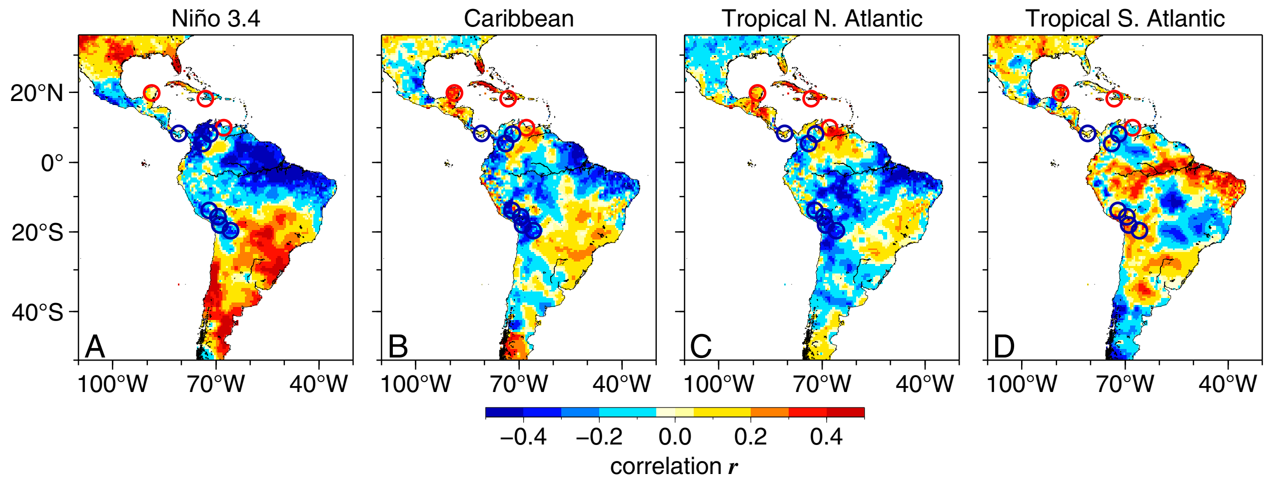

Fig. 4. Correlation between gridded precipitation over land (30) and SST time series for (*A*) the Niño 3.4 index, (*B*) the Caribbean, (*C*) the tropical north Atlantic, and (*D*) the tropical south Atlantic (regions defined in Fig. S5). Circles indicate paleorecords with a dry middle Holocene (blue) or wet middle Holocene (red). The Niño 3.4 spatial pattern is the most compatible with the compiled paleoclimate records, especially the coherence between northern and southern Andean sites and the site in central Panama. Although the Caribbean spatial pattern explains the similar response in lowland Venezuela and Haiti, it does not explain the phasing of the central Panamanian site. Additionally, the Caribbean pattern includes a significant component from the lagged effect of ENSO on Caribbean SSTs and precipitation (50) that is not accounted for in these instantaneous (lag 0) correlation maps. Both the tropical north and south Atlantic patterns fail to predict coherency between the southern Andes, northern Andes, and the Panamanian site.

northern and southern Andean sites for both the northern and southern tropical Atlantic sectors (Fig. 4). The correlation of precipitation with Caribbean SSTs is more similar to that for the Niño 3.4 region. However, the strength of the correlation is weaker in the Venezuelan Andes, and the sign of the correlation is opposite for the Panamanian site that is in-phase with the Venezuelan Andes over the Holocene, cases that are discussed below. Caribbean and Niño 3.4 SST time series are also significantly correlated ($r = 0.39$, $P = 0.004$) due to ENSO influences on the former, thus explaining a portion of the shared variance. When mapped, these correlations suggest that Caribbean and tropical Atlantic SSTs are unable to synchronize interhemispheric climate variability in the Andes, conferring the dominant role to equatorial Pacific SSTs.

Holocene Climate in the Neotropics. Coherent paleoclimate changes in a number of neotropical regions further supports the proposed role of equatorial Pacific forcing of South American climate. Holocene terrestrial records in Colombia, Venezuela, Panama, Mexico, and Bolivia are largely coherent with the Laguna Blanca record (11, 12, 21, 31–33). Moreover, the phasing of these Holocene records corresponds to the sign of their modern relationship with equatorial Pacific SSTs (Fig. 4) (24, 25, 28, 34, 35). For example, modern precipitation at Laguna Blanca and Lake Titicaca is negatively correlated with eastern equatorial Pacific SSTs and both lakes have the same, in-phase, Holocene lake-level history. Sites in-phase with Laguna Blanca (Fig. 3) include Lake La Yeguada (Panama) (32), Lake Fuquene (Colombian Andes) (33), and an array of lakes in the Bolivian Andes (17, 20, 21). Rainfall in all of these locations is negatively correlated with equatorial Pacific SSTs (Fig. 4) (24, 28, 34, 35). Sites that are antiphased with Laguna Blanca include Lake Valencia, Lake Cichancanab (Yucatan Peninsula, Mexico) (36, 37), and Lake Miragoane (Haiti) (38, 39). In each of these cases, precipitation correlates positively with equatorial Pacific SSTs, explaining their different responses relative to the Andean region. The relationship between modern precipitation variability and Holocene climate is evident even at the regional scale. For example, Lake Valencia and Laguna Blanca are less than 500 km from each other yet have opposite responses to ENSO (24, 25) and antiphased Holocene lake level histories (11, 12, 31)(Fig. 2).

Paleorecords of equatorial Pacific SSTs support this mechanism. Coral proxies and individual foraminiferal $\delta^{18}O$ both suggest that ENSO variability was reduced in the middle Holocene (40, 41), which would decrease moisture balance in the outer tropical Andes (Fig. S6). A continuous record of individual foraminiferal $\delta^{18}O$ variability suggests ENSO was similar to present during the early Holocene, reduced in strength or frequency during the middle Holocene (6–4 ka BP), and was near-modern levels during the late Holocene (42). These data provide an oceanic record of early Holocene ENSO variability, in agreement with the independent synthesis of terrestrial neotropical paleoclimate records presented here.

We surmise that precipitation in the outer tropics—especially the high Andes—is limited by the amount of moisture available for precipitation. Whereas the inner tropics of South America have abundant water vapor year-round, the outer tropics rely upon seasonal changes in wind patterns that deliver water vapor necessary for precipitation. These wind patterns are the mechanistic link between equatorial Pacific SSTs and local precipitation (25, 28), and aptly explain why the outer tropics appear strongly influenced by Pacific Ocean forcing. In contrast, insolation anomalies have a larger effect on the inner tropics by increasing the energy and large-scale dynamics that promote deep convection. The stronger influence from insolation explains why lake, ice core, and speleothem records in the central Andes (Peru, Ecuador) and the Amazon basin all exhibit secular $\delta^{18}O$ declines since the early Holocene, interpreted as increasing Amazonian precipitation, decreasing evaporation, and enhanced discharge in the Amazon basin (1–8). The pattern of increasing rainout of Amazon moisture is expressed in isotopic records throughout the tropical Andes, although much of this signal is inherited from upstream rather than local climate events (5, 43).

Conclusion

Our findings suggest that the prediction of insolation-driven, antiphased, Holocene climate evolution between the hemispheres is insufficient to account for the paleoclimate trends observed across all regions of South and Central America, particularly in the northern tropics. Instead we conclude that the equatorial Pacific played a far greater role than previously identified in modulating Holocene climate in the outer tropical

Andes. The analysis of modern coupled ocean-atmosphere variability in the tropics, including the dynamics of ENSO, offers viable mechanisms that reconcile the apparent synchroneity of these interhemispheric climate trends. Furthermore, our analysis underscores the potential for far more rapid climate shifts driven by variability of the mean state of tropical Pacific SSTs than would be possible by insolation forcing alone. The large range of future projections for equatorial Pacific variability under global warming scenarios (44) highlights the utility and importance of understanding past variability, the rate of change, and teleconnections. Our findings suggest that any sustained shift in the SST field of this region may portend abrupt hydrological shifts in parts of the Americas—including severe droughts or pluvial events analogous to those witnessed in the Middle Holocene. Today the equatorial Pacific plays a major role in the variability of water resources in regions of Australia, Indonesia, India, southeast Asia, the Americas, and parts of Africa (45). Future hydrologic variability in these regions may also be tied to the ocean-atmosphere response of the tropical Pacific in a warming world with a nonlinear or threshold response that should be carefully evaluated.

Materials and Methods

Overlapping sediment cores were recovered from the deepest part of Laguna Blanca using a square-rod coring system (46). AMS radiocarbon dates on terrestrial macrofossils constrain the age–depth relationship for the cores. Radiocarbon ages were calibrated using the IntCal04 dataset (Table S1) (47, 48) and interpolated linearly to construct an age model (Fig. S3). Unless otherwise noted, all ages in the manuscript refer to calibrated or calendar ages before AD 1950 (BP).

Dry sediment density was determined on 1 cm^3 core samples that were subsequently heated at 500 °C to determine total organic matter by mass loss (49). Volume MS was measured at 0.25 cm intervals on split cores using a Tamiscan automated sediment track and a Bartington high-resolution surface-scanning sensor connected to a susceptibility meter (reported in 10^{-6} SI units). Total organic carbon, total nitrogen, and C/N molar ratios were measured on decarbonated sediments (acetic acid/acetate buffer at pH 4) with a Costech CHNS elemental analyzer. Principal components analysis and correlations with water depth were carried out in MATLAB (*SI Text*).

ACKNOWLEDGMENTS. Meagan Mazzarino helped conduct the fieldwork. Helpful comments from two anonymous reviewers greatly strengthened the manuscript. Funding for this research was provided by the National Science Foundation Earth System History program (98-09472), the Geological Society of America, the Natural Sciences and Engineering Research Council of Canada, and the Department of Geosciences, University of Massachusetts.

1. Maslin MA, Burns SJ (2000) Reconstruction of the Amazon Basin effective moisture availability over the past 14,000 years. *Science* 290(5500):2285–2287.
2. Seltzer G, Rodbell DT, Burns S (2000) Isotopic evidence for late Quaternary climatic change in tropical South America. *Geology* 28(1):35–38.
3. Cruz FW, Jr., et al. (2005) Insolation-driven changes in atmospheric circulation over the past 116,000 years in subtropical Brazil. *Nature* 434(7029):63–66.
4. Ramirez E, et al. (2003) A new Andean deep ice core from Nevado Illimani (6350 m), Bolivia. *Earth Planet Sci Lett* 212:337–350.
5. Polissar PJ, Abbott MB, Shemesh A, Wolfe AP, Bradley RS (2006) Hydrologic balance of tropical South America from oxygen isotopes of lake sediment opal, Venezuelan Andes. *Earth Planet Sci Lett* 242:375–389, 10.1016/j.epsl.2005.12.024.
6. Wang X, et al. (2007) Millennial-scale precipitation changes in southern Brazil over the past 90,000 years. *Geophys Res Lett* 34, 10.1029/2007GL031149.
7. van Breukelen MR, Vonhof HB, Hellstrom JC, Wester WCG, Kroon D (2008) Fossil dripwater in stalagmites reveals Holocene temperature and rainfall variation in Amazonia. *Earth Planet Sci Lett* 275(1-2):54–60.
8. Thompson LG, et al. (1995) Late glacial stage and holocene tropical ice core records from Huascaran, Peru. *Science* 269(5220):46–50.
9. Cruz FW, et al. (2009) Orbitally driven east-west antiphasing of South American precipitation. *Nat Geosci* 2(3):210–214.
10. Haug GH, Hughen KA, Sigman DM, Peterson LC, Röhl U (2001) Southward migration of the intertropical convergence zone through the Holocene. *Science* 293(5533):1304–1308.
11. Bradbury JP, et al. (1981) Late quaternary environmental history of Lake Valencia, Venezuela. *Science* 214(4527):1299–1305.
12. Curtis JH, Brenner M, Hodell DA (1999) Climate change in the Lake Valencia Basin, Venezuela, approximately 12,500 yr BP to present. *Holocene* 9(5):609–619.
13. Martinez NC, et al. (2007) Modern climate forcing of terrigenous deposition in the tropics (Cariaco Basin, Venezuela). *Earth Planet Sci Lett* 264(3-4):438.
14. Martinez NC, et al. (2010) Local and regional geochemical signatures of surface sediments from the Cariaco Basin and Orinoco Delta, Venezuela. *Geology* 38(2):159–162, 10.1130/g30487.1.
15. Polissar PJ, et al. (2006) Solar modulation of Little Ice Age climate in the tropical Andes. *Proc Natl Acad Sci U S A* 103(24):8937–8942, 8910.1073/pnas.0603118103.
16. Alley RB, Ágústsdóttir AM (2005) The 8k event: Cause and consequences of a major Holocene abrupt climate change. *Quat Sci Rev* 24(10-11):1123–1149, 10.1016/j.quascirev.2004.12.004.
17. Tapia PM, Fritz SC, Baker PA, Seltzer GO, Dunbar RB (2003) A Late Quaternary diatom record of tropical climatic history from Lake Titicaca (Peru and Bolivia). *Palaeogeography, Palaeoclimatology, Palaeoecology* 194:139–164, 10.1016/s0031-0182(03)00275-x.
18. Abbott MB, Binford MW, Brenner M, Kelts KR (1997) A 3500 C-14 yr high-resolution record of water-level changes in Lake Titicaca, Bolivia/Peru. *Quat Res* 47:169–180.
19. Cross SL, Baker PA, Seltzer GO, Fritz SC, Dunbar RB (2000) A new estimate of the Holocene lowstand level of Lake Titicaca, and implications for Tropical Paleohydrology. *Holocene* 10(1):21–32.
20. Rowe HD, et al. (2003) Late Quaternary lake-level changes constrained by radiocarbon and stable isotope studies on sediment cores from Lake Titicaca, South America. *Global Planet Change* 38:273–290.
21. Abbott MB, et al. (2003) Holocene paleohydrology and glacial history of the central Andes using multiproxy lake sediment studies. *Palaeogeogr Palaeoclimatol Palaeoecol* 194:123–138, 10.1016/S0031-0182(03)00274-8.
22. Abbott MB, Seltzer GO, Kelts KR, Southon J (1997) Holocene Paleohydrology of the Tropical Andes from Lake Records. *Quat Res* 47:70–80.
23. Aceituno P (1988) On the functioning of the southern oscillation in the South American sector. Part I: Surface climate. *Mon Weather Rev* 116:505–524.
24. Pulwarty RS, Barry RG, Riehl H (1992) Annual and seasonal patterns of rainfall variability over Venezuela. *Erdkunde* 46:273–289.
25. Garreaud RD, Vuille M, Compagnucci R, Marengo J (2009) Present-day South American climate. *Palaeogeography, Palaeoclimatology, Palaeoecology* 281(3-4):180–195, 110.1016/j.palaeo.2007.1010.1032.
26. Polissar PJ (2005) *Lake Records of Holocene Climate Change, Cordillera de Mérida, Venezuela*. PhD dissertation (Univ of Massachusetts, Amherst, MA).
27. Rowe HD, Dunbar RB (2004) Hydrologic-energy balance constraints on the Holocene lake-level history of lake Titicaca, South America. *Clim Dyn* 23(3):439–454, 10.1007/s00382-004-0451-8.
28. Vuille M (1999) Atmospheric circulation over the Bolivian Altiplano during dry and wet periods and extreme phases of the Southern Oscillation. *Int J Climatol* 19:1579–1600.
29. Garreaud RD, Vuille M, Clement AC (2003) The climate of the Altiplano: Observed current conditions and mechanisms of past changes. *Palaeogeogr Palaeoclimatol Palaeoecol* 194:5–22.
30. Legates DR, Willmott CJ (1990) Mean seasonal and spatial variability in gauge-corrected, global precipitation. *Int J Climatol* 10(2):111–127, 10.1002/joc.3370100202.
31. Xu Y, Jaffé R (2008) Biomarker-based paleo-record of environmental change for an eutrophic, tropical freshwater lake, Lake Valencia, Venezuela. *J Paleolimnol* 40(1):179–194, 10.1007/s10933-007-9150-x.
32. Bush MB, Colinvaux PA (1990) A pollen record of a complete glacial cycle from lowland Panama. *J Veg Sci* 1:105–118.
33. Vélez MI, Hooghiemstra H, Metcalfe S, Martínez I, Mommersteeg H (2003) Pollen- and diatom-based environmental history since the Last Glacial Maximum from the Andean core Fúquene-7, Columbia. *J Quaternary Sci* 18(1):17–30.
34. Giannini A, Cane MA, Kushnir Y (2001) Interdecadal changes in the ENSO teleconnection to the Caribbean and the North Atlantic oscillation. *J Clim* 14:2867–2879.
35. Poveda G, Waylen PR, Pulwarty RS (2006) Annual and inter-annual variability of the present climate in northern South America and southern Mesoamerica. *Palaeogeogr Palaeoclimatol Palaeoecol* 234(1):3–27, 10.1016/j.palaeo.2005.10.031.
36. Covich A, Stuiver M (1974) Changes in oxygen 18 as a measure of long-term fluctuations in tropical lake levels and molluscan populations. *Limnol Oceanogr* 19(4):682–691.
37. Hodell DA, Curtis JH, Brenner M (1995) Possible role of climate in the collapse of Classic Maya civilization. *Nature* 375:391–394.
38. Hodell DA, et al. (1991) Reconstruction of Caribbean climate change over the past 10,500 years. *Nature* 352:790–793.
39. Curtis JH, Hodell DA (1993) *An Isotopic and Trace Element Study of Ostracods from Lake Miragoane, Haiti: A 10,500 Year Record of Paleosalinity and Paleotemperature changes in the Caribbean. Climate Change in Continental Isotopic Records*, Geophysical Monograph (American Geophysical Union, Washington, D.C.), Vol 78, pp 135–152.
40. Tudhope AW, et al. (2001) Variability in the El Niño-Southern Oscillation through a glacial-interglacial cycle. *Science* 291(5508):1511–1517.
41. Koutavas A, deMenocal PB, Olive GC, Lynch-Stieglitz J (2006) Mid-Holocene El Niño-Southern Oscillation (ENSO) attenuation revealed by individual foraminifera in eastern tropical Pacific sediments. *Geology* 34(12):993–996.
42. Koutavas A, Joanides S (2012) El Niño-Southern Oscillation extrema in the Holocene and Last Glacial Maximum. *Paleoceanography* 27(4):PA4208, 10.1029/2012pa002378.
43. Vuille M, et al. (2012) A review of the South American Monsoon history as recorded in stable isotopic proxies over the past two millennia. *Climate of the Past* 8:1309–1321, 10.5194/cp-8-1309-2012.
44. Guilyardi E, et al. (2009) Understanding El Nino in ocean-atmosphere general circulation models: Progress and challenges. *Bull Am Meteorol Soc* 90(3):325–340.
45. Curtis S (2008) The El Niño-Southern Oscillation and global precipitation. *Geography Compass* 2(3):600–619, 610.1111/j.1749-8198.2008.00105.x.

46. Wright HE, Mann DH, Glaser PH (1984) Piston corers for peat and lake sediments. *Ecology* 65:657–659.
47. Stuiver M, Reimer PJ, Braziunas TF (1998) High-precision radiocarbon age calibration for terrestrial and marine samples. *Radiocarbon* 40:1127–1151.
48. Reimer PJ, et al. (2004) IntCal04. *Radiocarbon* 46:1029–1058.
49. Dean WE, Jr. (1974) Determination of carbonate and organic matter in calcareous sediments and sedimentary rocks by loss on ignition: Comparison with other methods. *J Sediment Petrol* 44(1):242–248.
50. Giannini A, Kushnir Y, Cane MA (2000) Interannual variability of Caribbean rainfall, ENSO and the Atlantic Ocean. *J Clim* 13:297–311.

Supporting Information

Polissar et al. 10.1073/pnas.1219681110

SI Text

SI Reconstructions of Continental Climate from the Cariaco Basin

The Cariaco Basin is a marginal tectonic basin located immediately north of the Cordillera de la Costa, Venezuela. Sediment records from this basin have been a cornerstone for arguments that climate is antiphased between the northern and southern hemispheres of South America on precession timescales.

Sediments in the basin alternate seasonally between a light-colored, biogenic, and carbonate-rich layer and a dark-colored, mineral-rich terrigenous layer (1). The light layers are generated during the northern hemisphere dry season (boreal winter) when strong trade winds induce upwelling of nutrient-rich waters that drive abundant marine algal production. Dark layers are generated during the terrestrial wet season when fluvial runoff delivers aluminosilicate-rich sediments and slackened trade winds reduce nutrient delivery and marine productivity. Proxies for terrigenous sediment concentration and sediment composition inferred from sediment color disagree on the direction and magnitude of climate changes during the Holocene (Fig. S1) (2–6). Cariaco Basin sediment trap studies indicate that terrigenous flux does not simply reflect coastal rainfall and that the better correlation between rainfall and terrigenous sediment concentration primarily reflects dilution from biogenic sediments (7). This and other studies suggest a more complicated control over terrigenous geochemical indicators in the Cariaco Basin record during the Holocene (8).

SI Study Site, Coring, and Chronology

Laguna Blanca [8.33°N, 71.78°W, 1,620 m above sea level (a.s.l.)] is a small (0.05 km^2), shallow (5.5 m deep) lake situated on the north slope of the Cordillera de Mérida in the Venezuelan Andes (Fig. S2). The lake water is acidic (pH = 5.9), highly dilute (58 $\mu S \cdot cm^{-1}$), and anoxic within 50 cm of the sediment–water interface (9). The bathymetry is a simple bowl with a single deep basin, no surface inflow, and a lake level currently 5 m below a conspicuous dry outflow channel. The 0.87 km^2 catchment is forested and contains an upstream dry lake that would drain into Laguna Blanca during wet intervals when sufficient precipitation is available. The watershed is situated in steep local topography above any regional aquifers, precluding regional groundwater input to the lake. There is no evidence of recent or past glaciation in the catchment, consistent with its location below both modern and Pleistocene glaciation limits (10, 11). Lake-water $\delta^{18}O$ and δD are enriched relative to modern precipitation and groundwater, and lie along an evaporation trend distinct from local and global meteoric water lines ($\delta^{18}O_{lake}$, −1.7 ‰; $\delta^{18}O_{precip}$, −7‰ Vienna Standard Mean Ocean Water) (9). Both the lack of surface outflow and enriched water isotopes indicate the lake is hydrologically closed and at present undergoes significant evaporative enrichment.

In 1999 we recovered overlapping sediment cores from the deepest part of Laguna Blanca using a square-rod coring system (12). Accelerator mass-spectrometry (AMS) radiocarbon dates on terrestrial macrofossils constrain the age–depth relationship for the cores. Radiocarbon ages were converted to calendar ages using the IntCal04 dataset (Table S1) (13, 14). The age model (Fig. S3) was constructed by linear interpolation between the calibrated ^{14}C ages.

The composite stratigraphy from Laguna Blanca is 482 cm long with sediments that vary from organic-rich to clastic-dominated. The base of the core dates to 11,000 cal·y before present (BP) and all radiocarbon ages are in stratigraphic order except the samples at 188.5 and 175 cm. The 175 cm age appears too old and is not included in the age model, because it produces an abrupt shift in sedimentation rates during a period in the core where the sediment lithology suggests low and constant sedimentation rates, with no evidence of an unconformity. The two deepest radiocarbon samples in the age model were measured on bulk sediment rather than terrestrial macrofossils and as such are considered maximum limiting ages (15).

The calibrated radiocarbon age from Laguna Brava (Table S1) is located immediately above a desiccation layer and dates the end of the desiccation event. This event has a correlative lithostratigraphic expression in the Laguna Blanca record.

SI Seasonal Insolation Forcing and Tropical Climate Evolution

It is possible that transition season insolation changes (Spring or Fall) could play a role in Venezuelan climate or elsewhere by altering precipitation during the early or late wet season in regions that express two wet seasons per year. However, this interpretation appears unlikely for two reasons. First, during the Holocene, decreased insolation in the northern hemisphere during March–April–May is balanced by increased insolation during September–October–November (Fig. S4) (16). Thus, any reduction in precipitation during the early part of the wet season would reasonably be balanced by an increase in the later part of the wet season. Second, insolation forcing during these transition seasons cannot explain the heterogeneous pattern of wet or dry changes that occur within the same hemisphere (and in some cases regionally). Thus, although transition season insolation is perhaps relevant to specific individual localities, it cannot explain the Holocene climate history at all of the sites in the same way as Pacific sea-surface temperature (SSTs).

SI Correlation of South American Precipitation with SSTs

Correlations of gridded precipitation products with various SST time-series were used to explore the influence of tropical Pacific, Atlantic, and Caribbean SSTs on South American climate. Mean annual SSTs from the Nino 3.4, Caribbean, north Atlantic, and south Atlantic regions (Fig. S5) were spatially correlated with South American rainfall from the University of Delaware gridded data product (17) (UDel precipitation v.2.01 provided by the National Oceanic and Atmospheric Administration's Earth System Research Laboratory, Physical Sciences Division, www.esrl.noaa.gov/psd/).

SI Influence of El Niño-Southern Oscillation Variability on South American Precipitation

The nonlinear response of precipitation to SST variability has a strong influence on precipitation in the Venezuelan and Bolivian Andes. In the Venezuelan and Bolivian Andes, cold SST events have larger precipitation anomalies compared with warm events (Fig. S6). This asymmetry means that SST variability (as opposed to the mean state) can significantly increase the long-term water budget of these regions due to the disproportionate precipitation increase during cold events. Thus, both the linear response to mean SST conditions and the nonlinear response to SST variability are important determinants of climate in these regions. Wetter conditions occur when eastern equatorial Pacific SSTs are reduced or SST variability increases.

SI Reconstructed Lake Level

Past lake levels were approximated by calculating leading principle components of sediment properties scaled to modern lake bathymetry. Principle component analysis (PCA) of sediment compositional parameters [loss-on-ignition, dry density, elemental carbon/nitrogen (C/N) ratios, and the mass accumulation rate of mineral sediments] yields a first axis that captures 76% of the variance and separates dense, rapidly accumulating, organic poor sediments from less dense, slowly accumulating, organic matter-rich sediments (Fig. S7). These differences reflect high and low lake levels, respectively. The middle lake depth of ~5 m corresponds to moderate bulk density, loss on ignition (LOI), C/N, and mass accumulation rates between 1,000–2,000 y BP (Fig. S8). The overflowing lake depth corresponds to the 10 m elevation of the spill point above the modern lake floor, as prescribed for the 0–500 and 9,000–11,000 y BP intervals. In this model, wetland deposits correspond to a water depth of ~1 m above the modern lake floor, represented by the 4,000–7,000 y BP interval.

1. Hughen KA, Overpeck JT, Peterson LC, Anderson RF (1996) The nature of varved sedimentation in the Cariaco Basin, Venezuela, and its palaeoclimatic significance. *Geol Soc Lond Spec Publ* 116(1):171–183.
2. Hughen KA, et al. (1998) Deglacial changes in ocean circulation from an extended radiocarbon calibration. *Nature* 391:65–68.
3. Hughen KA, Overpeck JT, Peterson LC, Trumbore S (1996) Rapid climate changes in the tropical Atlantic region during the last deglaciation. *Nature* 380:51–54.
4. Peterson LC, Haug GH, Hughen KA, Röhl U (2000) Rapid changes in the hydrologic cycle of the tropical Atlantic during the last glacial. *Science* 290(5498):1947–1951.
5. Haug GH, Hughen KA, Sigman DM, Peterson LC, Röhl U (2001) Southward migration of the intertropical convergence zone through the Holocene. *Science* 293(5533): 1304–1308.
6. Piper DZ, Dean WE, Jr. (2002) *Trace-Element Deposition in the Cariaco Basin, Venezuela Shelf, Under Sulfate-Reducing Conditions—A History of the Local Hydrography and Global Climate, 20 ka to the Present* (US Geological Survey, Denver, CO), pp 1–45.
7. Martinez NC, et al. (2007) Modern climate forcing of terrigenous deposition in the tropics (Cariaco Basin, Venezuela). *Earth Planet Sci Lett* 264(3-4):438.
8. Martinez NC, et al. (2010) Local and regional geochemical signatures of surface sediments from the Cariaco Basin and Orinoco Delta, Venezuela. *Geology* 38(2): 159–162, 10.1130/g30487.1.
9. Polissar PJ (2005) Lake records of Holocene climate change, Cordillera de Mérida, Venezuela. PhD dissertation (Univ of Massachusetts, Amherst, MA).
10. Schubert C (1974) Late Pleistocene Mérida Glaciation, Venezuelan Andes. *Boreas* 3(4): 147–151.
11. Stansell N, Polissar PJ, Abbott MB (2007) Last Glacial Maximum equilibrium-line altitude and paleo-temperature reconstructions for the Cordillera de Mérida, Venezuelan Andes. *Quaternary Research* 67:115–127, 110.1016/j.yqres.2006.1007.1005.
12. Wright HE, Mann DH, Glaser PH (1984) Piston corers for peat and lake sediments. *Ecology* 65:657–659.
13. Stuiver M, Reimer PJ, Braziunas TF (1998) High-precision radiocarbon age calibration for terrestrial and marine samples. *Radiocarbon* 40:1127–1151.
14. Reimer PJ, et al. (2004) IntCal04. *Radiocarbon* 46:1029–1058.
15. Abbott MB, Stafford TW (1996) Radiocarbon geochemistry of modern and ancient arctic lake systems, Baffin Island, Canada. *Quat Res* 45:300–311.
16. Berger A, Loutre MF (1991) Insolation values for the climate of the last 10 million years. *Quat Sci Rev* 10:297–317.
17. Legates DR, Willmott CJ (1990) Mean seasonal and spatial variability in gauge-corrected, global precipitation. *Int J Climatol* 10(2):111–127.

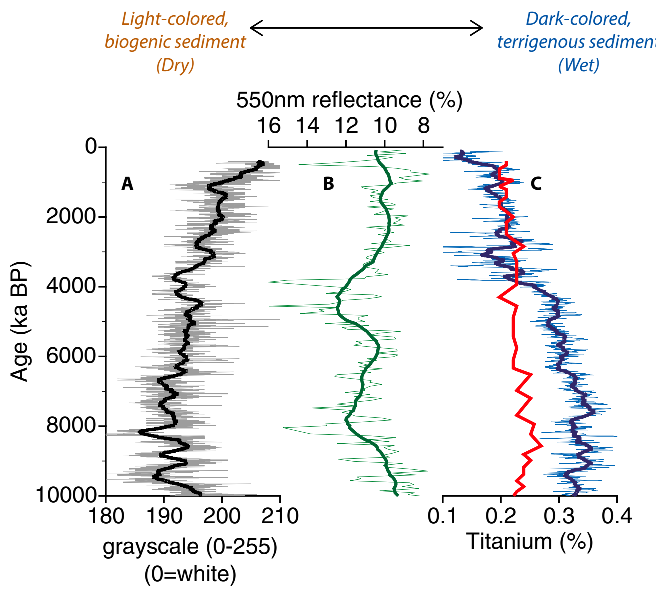

Fig. S1. Cariaco Basin sediment color and geochemistry. Grayscale (*A*, core PL07-56PC) (2, 3) and 550 nm reflectance (*B*, Ocean Drilling Program core ODP-1002C) (4) of Cariaco sediments indicates the contribution of light biogenic versus dark terrigenous sediment during the Holocene. Titanium concentrations measured by scanning X-ray fluorescence (*C*, blue line, core ODP-1002C) (5) and dissolution/inductively coupled plasma atomic emission spectroscopy (*C*, red line, core PL07-39PC) (6) reflect the concentration of terrigenous sediment. Disagreement between the reflectance records and the measured titanium concentrations suggests a more complicated proxy–climate relationship for these measurements than has been previously discussed.

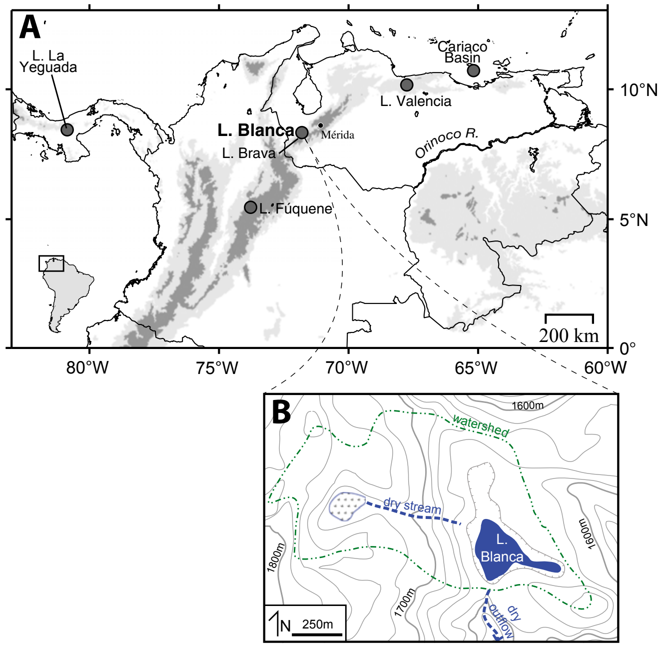

Fig. S2. Overview map showing Laguna Blanca and the location of other climate and paleoclimate records mentioned in the main text (*A*) and topography of the Laguna Blanca watershed (*B*). In *A*, Shading indicates elevations above 500 m (light gray) and 2000 m (dark gray).

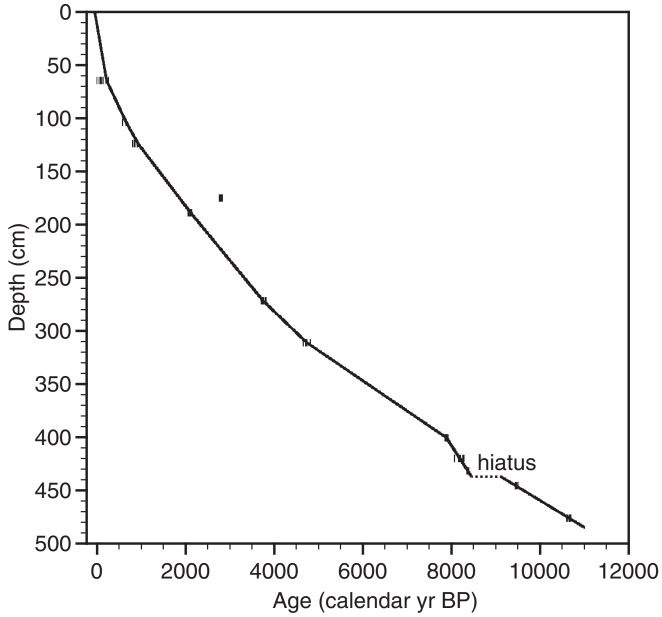

Fig. S3. Age–depth relationship for Laguna Blanca. The black bars indicate calibrated radiocarbon age ranges (1σ).

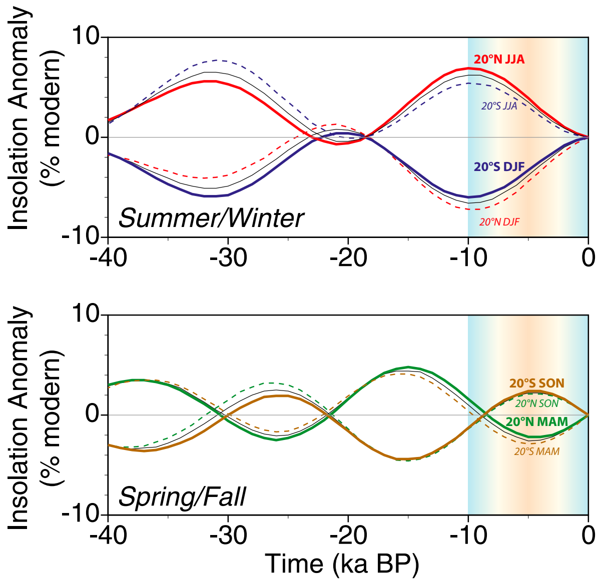

Fig. S4. Insolation anomalies for summer/winter and spring/fall (calculated from ref. 16).

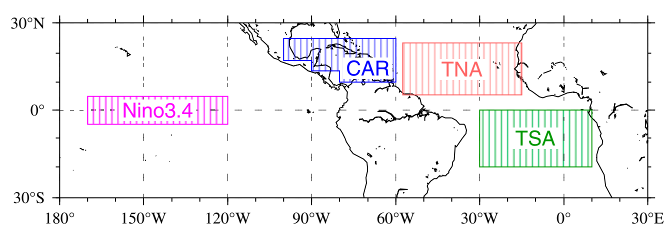

Fig. S5. Geographic regions defining the SST time-series.

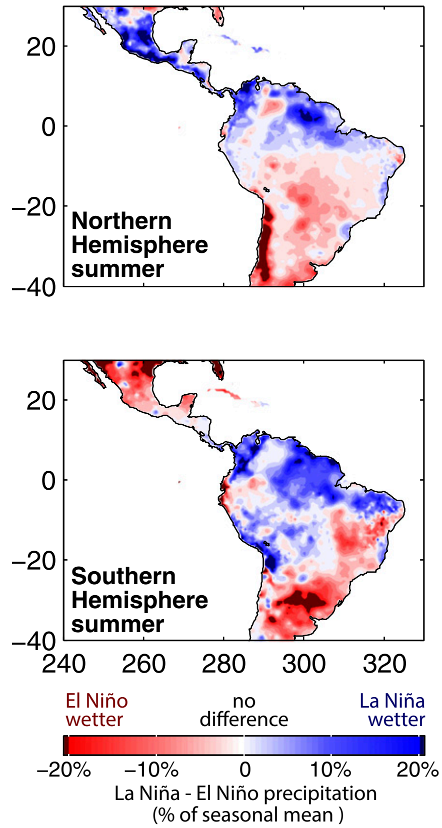

Fig. S6. Nonlinear impact of cold versus warm equatorial Pacific SSTs on South American precipitation. Shown is the wet season precipitation of the 10 coldest minus 10 warmest SST events between 1950–2000 A.D. as percentages of local mean wet-season precipitation. Strongly positive or negative anomalies (blue or red) indicate regions where El Niño-Southern Oscillation variability has a positive effect on local precipitation. In northern hemisphere summer (May–September), SST variability increases wet season precipitation in the Venezuelan Andes by almost 20%, whereas in southern hemisphere summer (November–March) precipitation in the region of Lake Titicaca increases by a corresponding amount. The October–December period of a 5-mo running average for Niño 3.4 SSTs was used to rank years. Precipitation anomalies from the University of Delaware Gridded Precipitation Product (v2.01) (17) are calculated for May–September of that year (northern hemisphere) and November–March of the following year (southern hemisphere).

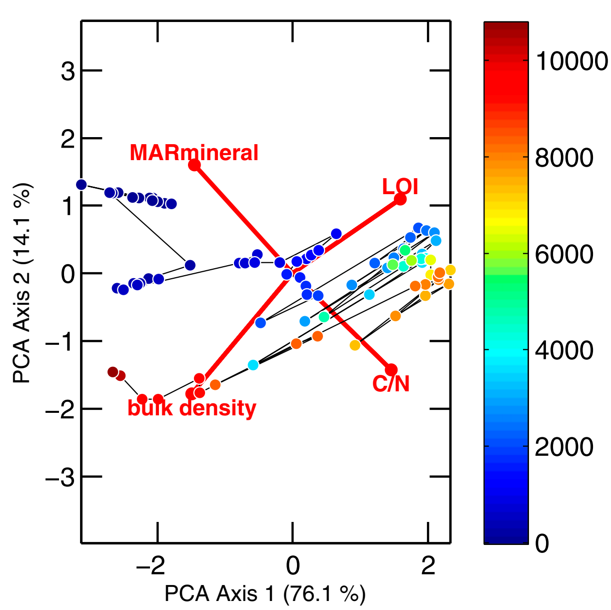

Fig. S7. PCA of sediment properties expressed as *z*-scores. Variable loadings are plotted with red lines and circles (3× magnitude for clarity), whereas sample scores are plotted with black lines and circles colored by sediment age. PCA axis 1 separates dense, high mineral mass accumulation rate sediments from those with high organic content and contributions from terrestrial organic matter.

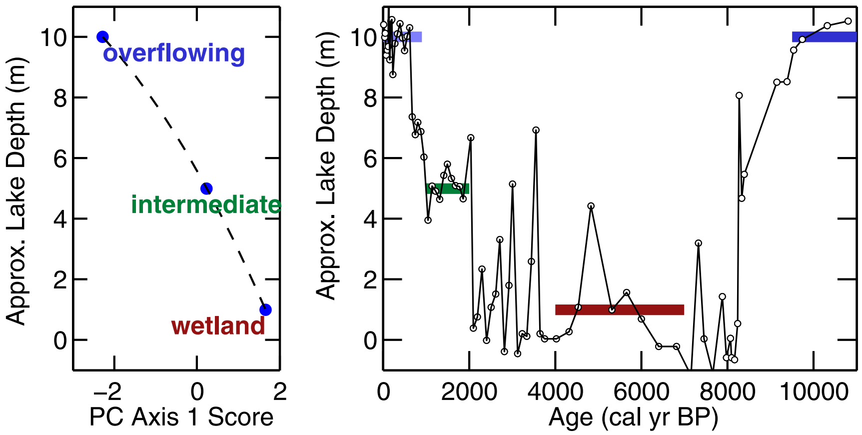

Fig. S8. PCA axis 1 scores were scaled to lake level (*Left*) based upon assumed intermediate lake levels 1,000–2,000 y BP, overflowing conditions during the early and late Holocene and low lake level with wetlands during the middle Holocene (*Right*).

Table S1. Radiocarbon ages (AMS) from Laguna Blanca core A-99 and Laguna Brava core A-97

Lake	Lab code	Drive	Drive depth, cm	Composite depth, cm	Material	^{14}C age	Calibrated age range, 1σ*
Blanca	CURL-4973	1	64.5	64.5	Wood	130 ± 35	−2–−1
							14–38
							64–118
							124–147
							189–193
							213–231
							243–268
Blanca	CURL-4974	2	13.5	103.5	Leaf	660 ± 35	564–589
							641–666
Blanca	CAMS-73134	2	33.5	123.5	Wood	980 ± 40	799–813
							826–866
							901–934
Blanca	CAMS-96801†	2	85	175.0	Wood	2,700 ± 60	2,757–2,849
Blanca	CAMS-96802	3	11	188.6	Wood	2,120 ± 35	2,044–2,147
Blanca	CAMS-96803	3	90	271.7	Wood	3,480 ± 40	3,698–3,734
							3,741–3,777
							3,789–3,827
Blanca	CAMS-96804	4	21.5	310.7	Wood	4,200 ± 35	4,652–4,669
							4,704–4,757
							4,809–4,836
Blanca	CAMS-96805	5	30.25	400.3	Wood	7,055 ± 40	7,850–7,907
							7,914–7,938
Blanca	CURL-4975	6	12	419.9	Wood	7,370 ± 45	8,060–8,087
							8,159–8,216
							8,242–8,304
Blanca	CAMS-96806	6	23.5	431.3	Wood	7,550 ± 45	8,344–8,403
Blanca	CAMS-96807	6	38	445.6	Bulk	8,430 ± 50	9,429–9,502
							9,508–9,517
Blanca	UCI-23056	7	17.5	476.0	Bulk	9,430 ± 40	10,589–10,630
							10,646–10,708
Brava‡	OS-18091	5	34	862	Wood	7,610 ± 50	8,375–8,445

*Based upon the intcal04 accessed at calib.qub.ac.uk on 4/20/2006.
†Not included in age model.
‡Sample from directly above desiccation layer in Laguna Brava.